AIAA JOURNAL
Vol. 45, No. 9, September 2007

Energy-Deposition/Extraction Effects on Oblique Shock Waves Over a Wedge

Chunpei Cai*
ZONA Technology, Scottsdale, Arizona 85258
and
Xin He†
Hong Kong University of Science and Technology,
Clear Water Bay, Kowloon, Hong Kong, People's Republic of China

DOI: 10.2514/1.28920

This paper reports some recent progress in analyzing the effects of an energy-deposition or extraction layer on supersonic flows over a wedge. Several algebraic relations across an energy-deposition/extraction layer are obtained, based on a quite simple model for the deposition/extraction layer. With the aid of these simple relations, we find analytical relations between the deposition/extraction and the pressure on the wedge apex point for two situations in which an oblique shock originally detaches from or attaches to the wedge apex point. This study obtains two important conclusions: For originally detached oblique shock waves, energy deposition results in a decrease in the pressure behind the shock and that on the apex point; energy extraction has the opposite effects. For originally attached oblique shock waves, energy deposition results in an increase in the pressure behind the shock and that on the apex point; with stronger energy deposition, the shock then detaches from the wedge and the pressure on the apex point begins to decrease. Two series of numerical simulations with Euler equations for flows over two 15- and 60-deg wedges with different energy-deposition/extraction strengths confirm the preceding conclusions.

Nomenclature

e	=	total energy per unit volume, $p/(\gamma-1)+(\rho u^2/2)$
L	=	energy-deposition/extraction zone length
M	=	Mach number
p	=	pressure
p_0	=	total pressure
$q, \dot{Q}$	=	energy-deposition/extraction strength
R	=	universal gas constant
T	=	temperature
u	=	velocity
α	=	semiapex angle for a wedge
β	=	oblique shock wave angle
γ	=	specific heat ratio, 1.4
ρ	=	density
σ	=	deposition/extraction strength parameter, $L\dot{Q}/(RT_1\sqrt{\gamma RT_1})$

Subscripts

1	=	preenergy-deposition/extraction region
2	=	postenergy-deposition/extraction region
3	=	point right behind a shock
4	=	wedge apex point

I. Introduction

ENERGY deposition for modification of the external flowfield around a vehicle is a well-known technique and has been studied and used to reduce the drag on objects flying at supersonic speeds. Since the 1950s, energy deposition in the supersonic flow was proposed as an alternative technique to reduce drag on flying objects [1]. Many papers discuss the significant drag decrease by energy deposition in front of an object, and analytical, numerical, and experimental studies were reported. Schneider et al. [2] reviewed steady and unsteady supersonic flow controls with energy addition in front of shock waves. More generally, Bushnell [3] reviewed the past and current shock wave drag-reduction techniques. Russian scientists performed a large amount of original work on this topic, however, many of their publications were in Russian and not conveniently accessible. Recently, several papers [4–16] about physical implementation, or numerical simulations of body control, or drag and heat exchange by localized energy addition in front of a shock wave were reported. The heat deposition is achieved by many different means, such as hot gas, laser beams, ultraviolet light, or electric arc and plasma beams.

Many energy-deposition applications share the same flowfield structure: in front of a shock wave, energy is deposited within a finite size area and it results in large pressure changes behind the shock wave. This paper aims to analytically study two simplified yet related two-dimensional problems, shown in Fig. 1. For case A, the shock originally detaches from a wedge, whereas for case B, the shock originally attaches to the wedge apex. A certain amount of energy is deposited into or extracted out of the flowfield, with a strength of $\dot{Q}$ and a region with width L. The height of the energy-deposition/extraction region is infinitely long to simplify the problem; a finite height represents a more realistic, but more difficult, problem. There are four regions in the flowfield for case A: the predeposition region 1, the preshock and postdeposition region 2, the postshock point 3, and the apex point 4. Between regions 1 and 2, energy is deposited/extracted with a strength of $\rho\dot{Q}$. The properties in regions 1 and 2 can be considered constant. For case B, the postshock point 3 and the apex point originally have the same location with an attached shock; when the energy deposition is strong, the shock detaches from the wedge and points 3 and 4 become different. This problem is close to such a physical situation: In a wind tunnel, supersonic gas passes a blunt or a sharp wedge that is located at the test section. By heating/cooling a narrow section of the tunnel right in front of the test section, we are about to investigate the property changes on the wedge apex point. This study is an extension of a simpler problem [17].

Received 17 November 2006; revision received 16 March 2007; accepted for publication 19 March 2007.

*Computational Fluid Dynamics Specialist, 9489 East Ironwood Square Drive, AIAA Senior Member.
†Visiting Research Scientist, Department of Mathematics.

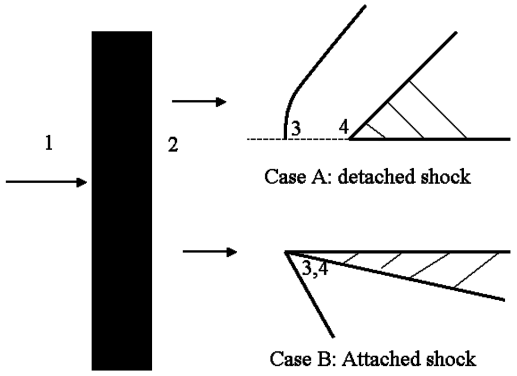

Fig. 1 Illustration of the flow problems.

This paper aims to obtain the analytical relations between the preshock energy-deposition/extraction effects and the properties on apex point 4. The pressure changes on the apex point with the energy deposition or extraction are of special concern. To the authors' knowledge, there is no previous study in the literature on this problem. It is expected that these relations can provide some insights to the more realistic situation of a finite height for the energy-deposition region.

II. Analytical Solutions and Discussions

A. Energy-Deposition/Extraction Region Relations

With an aim to obtain analytical solutions, we select the Euler equations and neglect the gas viscosity and thermal conductivity. The one-dimensional governing equations with energy deposition/extraction are [18]

$$p = \rho RT \qquad d(\rho u)/\,\mathrm{d}x = 0, \qquad d(p + \rho u^2)/\,\mathrm{d}x = 0$$
$$d(pu + eu)/\,\mathrm{d}x = \rho \dot{q} \tag{1}$$

As stated earlier, the right-hand side of the energy equation is zero everywhere in the flowfield, except between regions 1 and 2, in which it has a constant value of $\rho\dot{Q}$.

For a steady flow with a stationary planar shock wave, the preceding equations reduce to several simple algebraic relations. Especially, the energy equation can be simplified as

$$\gamma p_1 u_1/(\gamma - 1) + \rho_1 u_1^3/2 + \rho_1 \dot{Q} L = \gamma p_2 u_2/(\gamma - 1) + \rho_2 u_2^3/2$$
$$= \gamma p_3 u_3/(\gamma - 1) + \rho_3 u_3^3/2$$

with an assumption that across the short deposition/extraction layer, the density maintains a constant of ρ_1.

We define a nondimensional parameter $\sigma = L\dot{Q}/(RT_1\sqrt{\gamma RT_1})$ to represent the energy-deposition/extraction strength. Then from the preceding algebraic relations, the following simple relation between ρ_1 and ρ_2 exists:

$$\frac{\gamma + 1}{2(\gamma - 1)}\gamma M_1^2\left(\frac{\rho_1}{\rho_2}\right)^2 - \left(\frac{\gamma}{\gamma - 1} + \frac{\gamma^2 M^2}{\gamma - 1}\right)\frac{\rho_1}{\rho_2}$$
$$+ \left(\frac{\gamma}{\gamma - 1} + \frac{\gamma M_1^2}{2} + \frac{\sigma}{M_1}\right) = 0 \tag{2}$$

With the compatible relation that $\rho_1 = \rho_2$ when $\sigma = 0$, the following root of Eq. (2) is the correct relation between ρ_1 and ρ_2:

$$\rho_1/\rho_2 = (\gamma + \gamma^2 M_1^2 + A)/[(\gamma + 1)\gamma M_1^2] \tag{3}$$

where

$$A = \sqrt{(\gamma + \gamma^2 M_1^2)^2 - 2[\gamma/(\gamma - 1) + \gamma M_1^2/2 + \sigma/M_1](\gamma^2 - 1)\gamma M_1^2}$$

The other root is discarded because it yields a negative value for ρ_2 when $\sigma = 0$.

The other relations between regions 1 and 2 are

$$p_2/p_1 = (\gamma M_1^2 + 1 - A)/(\gamma + 1) \tag{4}$$

$$T_2/T_1 = \frac{(\gamma + \gamma^2 M_1^2 + A)}{(\gamma + 1)\gamma M_1^2}\frac{(\gamma M_1^2 + 1 - A)}{\gamma + 1} \tag{5}$$

$$M_2^2/M_1^2 = (\gamma + \gamma^2 M_1^2 + A)/[\gamma M_1^2(\gamma M_1^2 + 1 - A)] \tag{6}$$

It can be shown that the energy deposition or extraction cannot be infinitely strong. On one limit, A needs to be a real number, on the other limit, p_2 should be greater than zero. These two relations lead to the following relation:

$$\sigma_{\min} = (\gamma - 1 - 2\gamma M_1^2)/[2(\gamma - 1)\gamma M_1]$$
$$< \sigma < [\gamma(M_1^2 - 1)^2]/[2M_1(\gamma^2 - 1)] = \sigma_{\max} \tag{7}$$

The scope for energy deposition is much wider than that for energy extraction with $\sigma_{\max} \gg |\sigma_{\min}|$. When $\sigma = 0$, regions 1 and 2 have the same properties; whereas with the maximum energy deposition, $\rho_2/\rho_1 = (\gamma + 1)M_1^2/(1 + \gamma M_1^2)$, $p_2/p_1 = (\gamma M_1^2 + 1)/(\gamma + 1)$, $T_2/T_1 = (1 + \gamma M_1^2)^2/[(\gamma + 1)^2 M_1^2]$, and $M_2 = 1$. The maximum energy-deposition value is slightly different from previous results of Georgievskii et al. [4], because the definition of σ was different, and a Gaussian distribution for the energy deposition, extending to an infinite distance in front of the shock wave, was assumed in their paper. Meanwhile, Eq. (7) indicates that there is also a critical value for the energy extraction situation.

If the density for the right-hand-side term of the energy equation is not set to ρ_1, instead, more accurately, to $(\rho_1 + \rho_2)/2$, then the following complex relation can be obtained, which has quite complex solutions:

$$\left(\frac{\rho_1}{\rho_2}\right)^3 - \frac{2 + 2\gamma M_1^2}{M_1^2(\gamma + 1)}\left(\frac{\rho_1}{\rho_2}\right)^2$$
$$+ \frac{2 + (\gamma - 1)M_1^2 + (\gamma - 1)\sigma/(\gamma M_1)}{(\gamma + 1)M_1^2}\left(\frac{\rho_1}{\rho_2}\right)$$
$$+ \frac{(\gamma - 1)\sigma}{\gamma M_1^3(\gamma + 1)} = 0 \tag{8}$$

It is worthy to mention that all properties across the deposition/extraction layer are completely and explicitly determined by the nondimensional parameter σ and the incoming Mach number. This is crucial for the following discussions in the next two subsections.

We offer a comparison between our derivations from Eqs. (1–6) and those described otherwise [19], to conclude this subsection. Obviously, the discussions in the later reference are more general, accurate without any assumptions for the energy deposition, and the result formats are more concise than our results. However, it is very difficult to obtain an explicit expression for M_2/M_1 from Eq. (3.84) in [19]. With some sacrifice of accuracy by supposing $\rho = \rho_1$ for the energy input term, we obtain the explicit format of M_2/M_1 as Eq. (6). The exact formula of p_2/p_1, T_2/T_1, ρ_2/ρ_1, and p_{02}/p_{01} in [19] will be more complex if the exact format of M_2 is substituted; however, to obtain the format of M_2 from Eq. (3.84) in [19] is extremely difficult, if it is possible to solve it out.

B. Case A Results

With the deposition/extraction strength properly bounded, we can further compare its effect on the postshock properties, which is the major purpose of this study. If the shock originally detaches from the wedge, then from region 2 to point 3, the classical Rankine–Hugoniot relations hold, and from point 3 to point 4, the isentropic relations hold. All of the normal shock relations and isentropic relations can be found in many aerodynamics books [20]. For case A, the final relations between the stagnation point 4 and region 1 are

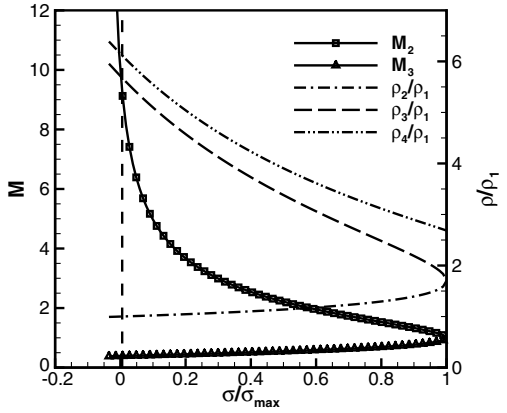

Fig. 2 Case A energy-deposition/extraction effects on Mach number and density results;$M_1 = 10.0$ and $\gamma = 1.4$.

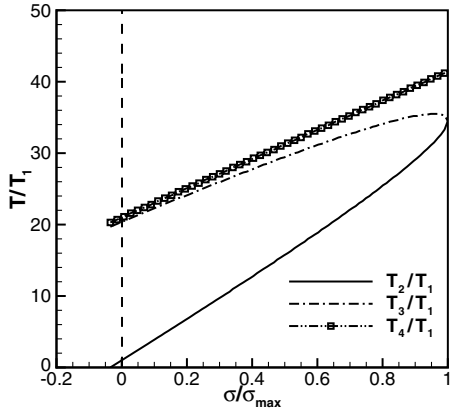

Fig. 3 Case A energy-deposition/extraction effects on temperature results; $M_1 = 10.0$ and $\gamma = 1.4$.

$$\frac{p_4}{p_1} = \left[\frac{2\gamma M_2^2 - (\gamma - 1)}{\gamma + 1}\right]\left(\frac{\gamma M_1^2 + 1 - A}{\gamma + 1}\right)\left(1 + \frac{\gamma - 1}{2} M_3^2\right)^{\gamma/(\gamma-1)} \tag{9}$$

$$\frac{\rho_1}{\rho_4} = \frac{\gamma + \gamma^2 M_1^2 + A}{(\gamma + 1)\gamma M_1^2}\left[\frac{2 + (\gamma - 1)M_2^2}{(\gamma + 1)M_2^2}\right]\left(1 + \frac{\gamma - 1}{2} M_3^2\right)^{-1/(\gamma-1)} \tag{10}$$

$$\frac{T_4}{T_1} = \left(\frac{[2\gamma M_2^2 - (\gamma - 1)][2 + (\gamma - 1)M_2^2]}{(\gamma + 1)^2 M_2^2}\right) \times \left[\frac{(\gamma + \gamma^2 M_1^2 + A)}{(\gamma + 1)\gamma M_1^2}\frac{(\gamma M_1^2 + 1 - A)}{\gamma + 1}\right]\left(1 + \frac{\gamma - 1}{2} M_3^2\right) \tag{11}$$

The energy-deposition or extraction effects on the pressure for case A can be obtained by

$$d(p_3/p_1)/\,\mathrm{d}\sigma = \frac{1}{\gamma + 1}\,\mathrm{d}A/\,\mathrm{d}\sigma < 0 \tag{12}$$

$$\frac{d(p_4/p_1)}{\mathrm{d}\sigma} = \frac{(1 + \gamma)^2}{2\gamma}\frac{A(1 + A + \gamma M_1^2)}{[2\gamma M_2^2 - (\gamma - 1)]^2}\frac{1}{(\gamma M_1^2 + 1 - A)^2} \times \left(1 + \frac{\gamma - 1}{2} M_3^2\right)^{1/(\gamma-1)}\frac{\mathrm{d}A}{\mathrm{d}\sigma} < 0 \tag{13}$$

Hence, for case A, for an energy-deposition situation with $d\sigma > 0$, the pressure behind the shock and on the wedge apex point decreases; for an energy extraction situation with $d\sigma < 0$, pressure increases. To discuss these analytical results, the preshock and postshock conditions versus the deposition/extraction strength are plotted with an incoming Mach number $M_1 = 10.0$ and $\gamma = 1.4$. In each of the following figures, a vertical dashed line represents the no-energy-deposition/extraction condition, and the intersection points with the other curves are the standard reference values.

Figure 2 shows the energy-deposition/extraction effects on the preshock and postshock Mach numbers and densities for case A. When the deposition strength increases, the preshock density increases and Mach number decreases rapidly, resulting in a weaker shock wave. When the deposition reaches its maximum value, the shock ceases to exist, and this maximum deposition value is a critical point. On the other hand, stronger extraction results in a decrease in the preshock density and an increase in the Mach number in front of the shock. Theoretically, it is very possible to create a hypersonic flow in the postextraction region. On the extraction limit, an infinitely large preshock Mach number is created and the postshock density reaches the hypersonic limit of 6. It is very evident that the window for extraction is much narrower than that for deposition.

Figure 3 shows the deposition/extraction effects on the static temperature and postshock stagnation temperature for case A. As the deposition strength increases, all the temperatures continue to increase, although continuing energy extraction eventually results in a zero preshock static temperature.

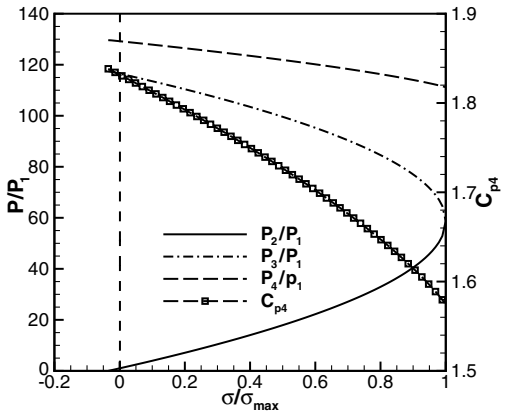

Fig. 4 Case A energy-deposition/extraction effects on pressure results; $M_1 = 10.0$ and $\gamma = 1.4$.

Figure 4 shows that for case A, stronger energy deposition results in a higher preshock pressure and lower postshock static and stagnation pressure, mainly due to a lower Mach number. Whereas, on the contrary, an energy extraction results in a higher postshock static pressure and a higher stagnation pressure.

C. Case B Results

For case B, the shock stays attached to the wedge with weak energy depositions. Across the shock wave, the oblique shock relations instead of the normal shock wave relations hold, and points 3 and 4 are the same point. With stronger energy depositions, the shock detaches from the wedge, and points 3 and 4 become different from then on; under that situation, the problem degenerates to case A and the formulas are the same as case A.

The most interesting result is the pressure change on the wedge apex point with energy deposition and extraction when the shock still attaches to the wedge:

$$\frac{d(p_3/p_1)}{\mathrm{d}\sigma} = -\frac{(\gamma - 1)\gamma M_1(\gamma - 1 + 2\sin^2\beta)}{(\gamma + 1)A} + \frac{4(\gamma + \gamma^2 M_1^2 + A)\sin\beta\cos\beta}{(1 + \gamma)^2}\frac{\mathrm{d}\beta}{\mathrm{d}\sigma} \tag{14}$$

$$\left.\frac{d(p_3/p_1)}{\mathrm{d}\sigma}\right|_{\sigma=0} = \mathcal{O}(-1/M_1) + \mathcal{O}(M_1^2)\,\mathrm{d}\beta/\,\mathrm{d}\sigma$$
$$\left.\frac{d(p_3/p_1)}{\mathrm{d}\sigma}\right|_{\sigma=\sigma_{\max}} = -\infty \tag{15}$$

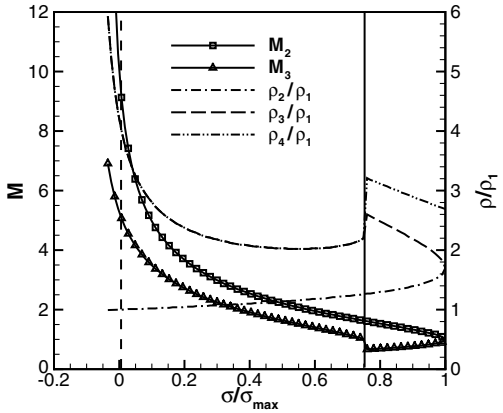

Fig. 5 Case B energy-deposition/extraction effects on Mach number and density results; $M_1 = 10.0$, and $\gamma = 1.4$.

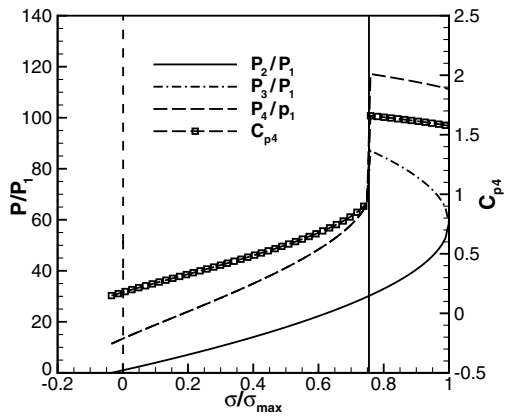

Fig. 7 Case B energy-deposition/extraction effects on pressure results; $M_1 = 10.0$ and $\gamma = 1.4$.

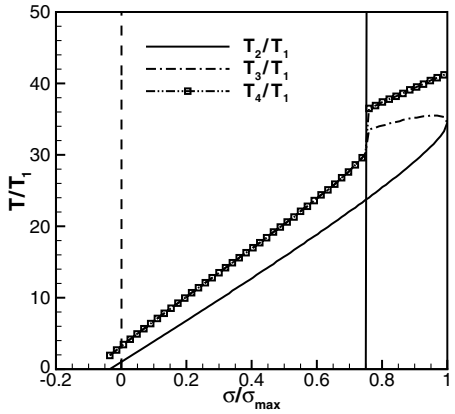

Fig. 6 Case B energy-deposition/extraction effects on temperature results; $M_1 = 10.0$ and $\gamma = 1.4$.

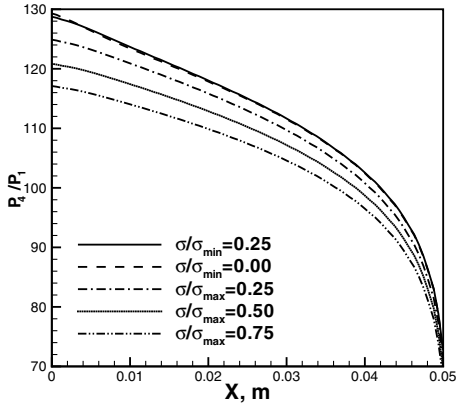

Fig. 8 Test case A energy-deposition/extraction effects on pressure profiles along the wedge surface; $M_1 = 10.0$, $\gamma = 1.4$, and $\alpha = 60$ deg.

where $A(\sigma = 0) = \gamma M_1^2 - \gamma$ and $A(\sigma = \sigma_{\max}) = 0$ are used to obtain Eq. (15) from Eq. (14). Considering the fact that stronger energy deposition (i.e., $\mathrm{d}\sigma > 0$) creates a lower preshock Mach number and hence a larger shock attach angle (i.e, $\mathrm{d}\beta > 0$), it is evident that $\mathrm{d}\beta/\mathrm{d}\sigma > 0$.

It is quite difficult to determine whether $d(p_3/p_1)/\mathrm{d}\sigma$ is larger or smaller than zero with Eq. (14); however, it is evident from Eq. (15) that with $\sigma = 0$, the value is positive with a large value of M_1 or a hypersonic incoming flow situation, but it becomes negative before the deposition reaches the maximum value. Hence, the pressure behind the shock can increase with energy deposition $d\sigma > 0$ if M_1 is strong enough and the shock still attaches to the wedge. The following figures further illustrate the results.

Figure 5 shows the energy-deposition and extraction effects on the preshock and postshock Mach numbers and densities for case B. A vertical solid line is added to illustrate the critical energy-deposition value for a shock detachment. When the deposition strength increases, the preshock density increases and the Mach number decreases rapidly, resulting in a weaker oblique shock wave. When the deposition reaches a critical value, the shock detaches from the wedge and forms a local normal shock wave. On the other hand, stronger extraction creates a decrease in the preshock density and an increase in the Mach number in front of the shock.

Figure 6 shows the deposition and extraction effects on the postshock static and stagnation temperatures for case B. The same conclusions as those from case A hold, with an additional abrupt change in the profiles when the shock detaches from the wedge.

Figure 7 shows that for case B, stronger energy deposition results in a higher preshock pressure and also a higher postshock static pressure and a higher stagnation pressure if the shock still attaches to the wedge. Only after the shock detaches from the wedge does the pressure on the apex and C_p begin to decrease. Energy extraction results in a lower postshock static pressure and a lower stagnation pressure.

Although it is reported in the literature that energy deposition in front of a wedge reduces the pressure drag, with the assumptions in this study, the current model and analytical results do not completely support these conclusions for the situations with the shock originally attaching to the wedge. We want to point out that a finite height for the deposition/extraction layer results in a different problem from that discussed in this study. A more advanced model with a finite length of deposition/extraction region and with inclusions of viscosity and heat conduction can probably provide better insights.

III. Numerical Simulations

To test the results from the last section, we perform two series of simulations by solving Euler equations. In these simulations, supersonic gas flows pass two wedges with a wedge semiangle of $\alpha = 15$ or 60 deg. For several computational cases, the shock waves detach from the wedge and a flat wedge shoulder is adopted to prevent an infinitely large detachment distance from the wedge. The simulations use a heat-deposition length of 0.02 m. The left side of the simulation domain uses an inlet boundary condition, the bottom side uses a symmetric boundary condition, the right side uses a wall boundary, and the top side uses an outflow boundary with $\partial(\,)/\partial n = 0$. The inlet boundary conditions are $M_\infty = 10.0$, $T_\infty = 300$ K, $p_\infty = 1.01325 \times 10^5$ Pa, and $\gamma = 1.4$. In the Euler equation solver, inviscid flux is computed with the classical Roe scheme.

Figure 8 shows the pressure distributions along the blunt wedge. The values are obtained from the pressure in the first layer of cells

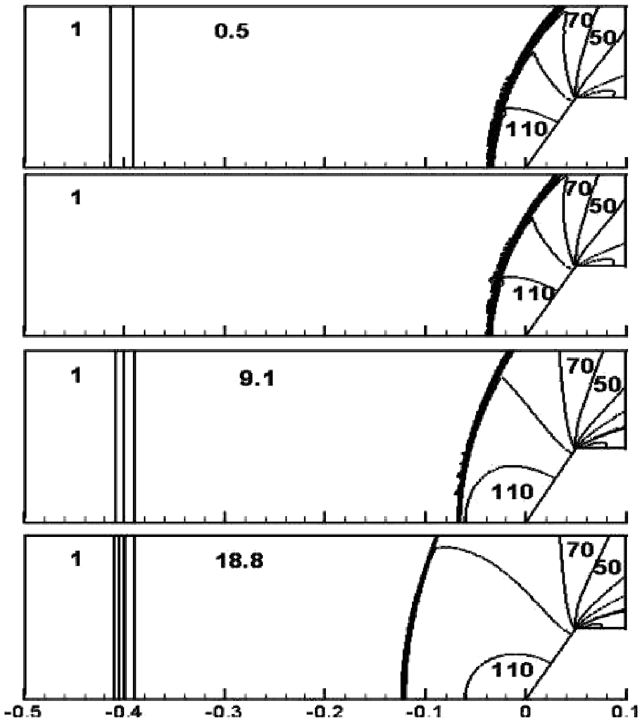

Fig. 9 Test case A energy-deposition/extraction effects on pressure contours; $M_1 = 10.0$, $\gamma = 1.4$, $\alpha = 60$ deg, $\sigma/\sigma_{\min} = 0.25$, and $\sigma/\sigma_{\max} = 0.0, 0.25$, and 0.75.

close to the wall. Because for case A the shock detaches from the wedge, each point on the wall surface has a different pressure value. For the stagnation point in which we are interested, with positive heat deposition in general, the pressure on the wall decreases, whereas with energy extraction, the pressure on the stagnation point slightly increases, matching our analytical results. Pressure distributions along the wedge shoulder are neglected. For the energy-extraction effect, the simulation is quite difficult for two reasons: $|\sigma_{\min}| \ll \sigma_{\max}$, hence the parameter window is much narrower, and as shown by Fig. 2, energy extraction creates hypersonic flows in the postextraction layer, and the strong shock wave gradients easily trigger a code failure.

Figure 9 shows the pressure contours with $\sigma/\sigma_{\min} = 0.25$ and $\sigma/\sigma_{\max} = 0.0, 0.25$, and 0.75, to illustrate the global effects of energy deposition or extraction. Note that the marked pressure values are approximate values; more accurate results should be obtained by careful probations. Obviously, as the energy-deposition strength increases, the shock standing-off distance becomes larger, reflecting a weaker shock wave, and the changes in the preshock pressure fit our analytical results.

Figure 10 shows that the wall pressure changes for gas passing the 15-deg wedge. The values are obtained from the pressure values on the first layer of cell center close to the wall. With zero heat deposition, the pressure in the first layer of cell is constant and actually fits the classical oblique shock wave solutions very well. For a small σ value situation, the first cell pressure is much lower than the rest of the data, because the shock is attached to the wedge and the first cell center is actually in front of the shock wave with a lower pressure value. This figure shows that as the deposition strength increases, the pressure on the wedge increases; with energy extraction, the pressure slightly decreases; and both match our analytical predictions. With $\sigma/\sigma_{\max} = 0.85$, the first pressure point is larger than the pressure in other cells, indicating that the shock detaches from the wedge. Figure 7 indicates that the detachment happens at $\sigma/\sigma_{\max} = 0.75$ for this incoming Mach number. It is not very clearly shown in Fig. 10, but we observe that the pressure in the first cell with $\sigma/\sigma_{\max} = 0.90$ is slightly smaller than that with $\sigma/\sigma_{\max} = 0.85$, also matching our analytical results. It is quite difficult to simulate flows with $\sigma/\sigma_{\max} = 0.90$, because with a

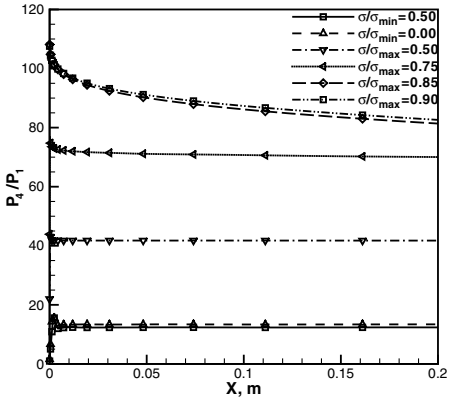

Fig. 10 Test case B energy-deposition/extraction effects on pressure profiles along the wedge surface; $M_1 = 10.0$, $\gamma = 1.4$, and $\alpha = 15$ deg.

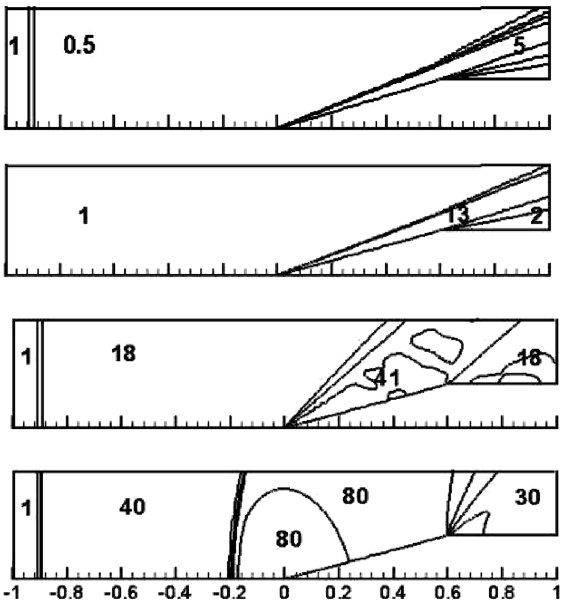

Fig. 11 Test case B energy-deposition/extraction effects on pressure contours; $M_1 = 10.0$, $\gamma = 1.4$, $\alpha = 15$ deg, $\sigma/\sigma_{\min} = 0.25$, and $\sigma/\sigma_{\max} = 0.0, 0.50$, and 0.75.

stronger deposition, maintaining the deposition layer in front of a detached shock wave requires larger simulation domains in the X direction.

Figure 11 shows the pressure contours with $\sigma/\sigma_{\min} = 0.25$ and $\sigma/\sigma_{\max} = 0.0, 0.50$, and 0.75. It is very evident that as the energy-deposition strength increases from 0.0 to $0.50\sigma_{\max}$, the shock still attaches to the wedge and the pressure on the wedge actually increases, matching the predictions from our analytical results in the previous section.

Hence, these two series of simulations confirm the important predictions from our analytical results.

IV. Conclusions

We reported an analysis of energy-deposition and extraction effects on the postshock pressure, with shocks originally detaching from or attaching to a wedge. The model used here neglected the viscosity and thermal conductivity effects and adopted an infinite height for the deposition or extraction layer. By solving the Euler equations, simple algebraic relations among the incoming flow, preshock, and postshock regions were obtained. The analytical results indicate that energy deposition results in an increase in the gas density in the postdeposition region and lower preshock Mach numbers, and with the critical energy-deposition value, the shock

ceases to exist. For an originally detached shock, stronger energy deposition in front of the shock results in a decrease in the postshock static pressure and the stagnation pressure; however, for originally attached shock waves, energy deposition results in a raise in the pressure on the apex point until the deposition is strong enough to create a detached shock wave. In general, for both cases, energy extraction yields the exact opposite effects as the energy deposition.

Acknowledgment

This work is partially supported by the Internal Research and Development funding from ZONA Technology.

References

[1] Oswatitsch, K., "Propulsion with Heating at Supersonic Speed," Deutsche Versuchsanstalt fur Luft und Raumfahrt, Rept. 90, Berlin, 1959.

[2] Schneider, M. N., Macheret, S. O., Zaidi, S. H., Girgis, I. G., Raizer, Yu. P., and Miles, R. B., "Steady and Unsteady Supersonic Flow Control with Energy Addition," 34th AIAA Plasmadynamics and Lasers Conference, Orlando, FL, AIAA Paper 2003-3862, 2003.

[3] Bushnell, D. M., "Shock Wave Drag Reduction," *Annual Review of Fluid Mechanics*, Vol. 36, 2004, pp. 81–96.

[4] Georgievskii, P. Yu, and Levin, V. A., "Control of the Flow Past Bodies Using Localized Energy Addition to the Supersonic Oncoming Flow," *Fluid Dynamics*, Vol. 38, No. 5, 2003, pp. 794–805.

[5] Georgievsky, P. Yu, and Levin, V. A., "Bow Shock Wave Structures Control by Pulse-Periodic Energy Input," 42nd AIAA Aerospace Sciences Meeting and Exhibit, Reno, NV, AIAA Paper 2004-1019, 2004.

[6] Luk'yanov, G. A., "Drag and Heat Exchange of an Object in a Supersonic Flow with a Planar Source of Energy in Front of the Object," *Technical Physics Letters*, Vol. 24, No. 12, 1998, pp. 980–982.

[7] Guvernyuk, S. V., and Samoilov, A. B., "Control of Supersonic Flow around Bodies by Means of a Pulsed Heat Source," *Technical Physics Letters*, Vol. 23, No. 5, May 1997, pp. 333–336.

[8] Kandala, R., and Candler, G., "Numerical Studies of Laser-Induced Energy Deposition for Supersonic Flow Control," 41st Aerospace Sciences Meeting and Exhibit, Reno, NV, AIAA Paper 2003-1052, 2003.

[9] Kremeyer, K., Sebastian, K., and Shu, C. W., "Computational Study of Shock Mitigation and Drag Reduction by Pulsed Energy Lines," *AIAA Journal*, Vol. 44, No. 8, Aug. 2006, pp. 1720–1731.

[10] Kremeyer, K., "Lines of Pulsed Energy for Supersonic/Hypersonic Drag Reduction: Generation and Implementation," 42nd AIAA Aerospace Sciences Meeting and Exhibit, Reno, NV, AIAA Paper 2004-0984, 2004.

[11] Ganiev, Y. C., Gordeev, V. P., Krasilnikov, A. V., Lagutin, V. I., Otmennikov, V. N., and Panasenko, A. V., "Aerodynamic Drag Reduction by Plasma and Hot-Gas Injection," *AIAA Journal*, Vol. 14, No. 1, Jan.–Mar. 2000, pp. 10–17.

[12] Latypov, A. F., and Fomin, V. M., "Evaluation of the Energy Efficiency of Heat Addition Upstream of the Body in a Supersonic Flow," *Journal of Applied Mechanics and Technical Physics*, Vol. 43, No. 1, 2002, pp. 59–62.

[13] Riggins, D., Nelson, H. F., and Johnson, E., "Blunt-Body Wave Drag Reduction Using Focused Energy Deposition," *AIAA Journal*, Vol. 37, No. 4, 1999, pp. 406–467.

[14] Meyer, B., Nelson, H. F., and Riggins, D. W., "Hypersonic Drag and Heat Transfer Reduction Using a Forward-Facing Jet," *Journal of Aircraft*, Vol. 38, No. 4, July–Aug. 2001, pp. 680–685.

[15] Yan, H., Adlgren, R., Elliott, G., Knight, D., and Beuther, T., "Effect of Energy Addition on MR-RR Transition," *Shock Waves*, Vol. 13, No. 1, 2003, pp. 113–121.

[16] Adelgren, R., Yan, H., Elliott, G. S., Knight, D., Beutner, T., and Zheltovodov, A. A., "Control of Edney IV Interaction by Pulsed Laser Energy Deposition," *AIAA Journal*, Vol. 43, No. 2, 2005, pp. 256–269.

[17] Cai, C., "Energy Deposition/Extraction Effects on a Planar Shock Waves," *Journal of Thermophysics and Heat Transfer*, Vol. 21, No. 1, Jan.–Feb. 2007, pp. 252–254.

[18] Zel'dovich, Ya. B., and Raizer, Yu. P., *Physics of Shock Waves and High-Temperature Hydrodynamic Phenomena*, edited by Hayes, W. D. and Probstein, R. F., Dover, New York, 2002.

[19] Anderson, J. D., *Modern Compressible Flow with Historical Perspective*, 3rd ed., McGraw–Hill, New York, 2003, Sec. 3.8, pp. 102–105.

[20] Saad, M. A., *Compressible Fluid Flow*, Prentice–Hall, Upper Saddle River, NJ, 1993.

X. Zhong
Associate Editor